Key Engineering Materials
ISSN: 1662-9795, Vol. 926, pp 331-340
doi:10.4028/p-uq57va

Submitted: 2021-12-08
Accepted: 2022-02-18
Online: 2022-07-22

Thermal Modeling of Laser Powder Bed Fusion During Printing on Temperature-Unstable Materials Considering Local Sintering

Felix Frölich[1,a*] and Luise Kärger[1,b]

Institute of Vehicle System Technology, Karlsruhe Institute of Technology (KIT), Germany

[a]felix.froelich@kit.edu, [b]luise.kaerger@kit.edu

Keywords: Selective Laser Melting, FEM, Powder Bed, Hybridization, Sintering, Thermal Conductivity, Abaqus

Abstract. The integration of local metal structures into polymer components using Laser Powder Bed Fusion (PBF-LB/M) offers great potential regarding multifunctional lightweight structures. However, such process hybridization involves huge challenges. In order to reduce the temperature input into the less temperature-resistant materials, the use of lower laser powers in the interfacial region is essential. The resulting local sintering of the metal powder affects the thermal properties in the interfacial region, leading to a change in heat dissipation in the temperature-unstable material. A modeling approach oriented to selective laser sintering is presented for predicting the degree of sintering and associated thermal properties in the context of PBF-LB/M process simulation.

Introduction

Laser Powder Bed Fusion (PBF-LB/M) process is one of the most industrially applied additive manufacturing technologies due to the associated geometry and design freedom as well as the reduction of lead time for development components [1, 2, 3]. Integration of local metal structures by the PBF-LB/M process into polymer components would allow a wide range of function integrations as well as a large design freedom of hybrid metal-polymer structures [4]. Accordingly, a process hybridization of metal and polymer-based additive manufacturing technologies holds much potential in terms of multifunctional lightweight structures.

The printing of polymers on metal structures has already been investigated and researched [4, 5, 6]. PBF-LB/M printing on comparatively less temperature-resistant materials, such as polymers, brings high challenges due to the high process temperatures and has therefore been marginally investigated so far. However, the process hybridization that can be fully realized in this way would allow hybrid components to be designed almost freely.

In order to be able to print on less temperature-resistant materials using a PBF-LB/M process, it is necessary to work with reduced laser powers in the area of the interface. This is the only way to avoid excessive energy input into the temperature-unstable material and thus its destruction. Since the resulting temperature in the metal must necessarily be lower than its liquidus temperature T_{L}, local sintering of the powder particles occurs in the area of the interfacial layers. It can be assumed that this locally different structure influences the thermophysical properties in the area of the interface [7] and is also decisive for the resulting mechanical properties of these boundary layers. Since such process hybridization has hardly been studied so far, a fundamental understanding of the process is essential. Numerical methods can contribute to this. Furthermore, an accurate prediction of the material state in the region of the interface is helpful to design the process control for optimal mechanical properties at acceptable energy input into the temperature-unstable interface.

In the literature, there are already some publications on the simulation of the PBF-LB/M process. For example, Xie et al. [8] and Zhang et al. [9] present models for the consideration of individual phases as well as their transitions during the melting process. However, since direct melting of the powder bed is aspired for during the manufacturing process and thus no sintered areas remain in the printed structure, the described models only represent the powder, melt and solid phases. Therefore, this paper presents an extension of this modeling approach based on selective laser sintering [7] to predict the

degree of sintering and to consider the associated thermal properties in the context of PBF-LB/M process simulation. Using an FE model of a single bead test with different laser powers per printed layer, the conventional PBF-LB/M modeling approach is compared with the approach presented here.The degree of sintering and the thermal conductivity in the interfacial layers as well as the heat input into the temperature-unstable material are discussed.

Thermal Modeling Approach

The governing equation for thermal modeling is the heat balance equation in combination with the generalized Fourier equation, which is given in weak form as follows:

$$\int_{\Omega} \rho c_{\mathrm{p}}(T)\dot{T}\delta T \,\mathrm{d}V = -\int_{\Omega} (\boldsymbol{\lambda}(T)\cdot \mathrm{grad}(T))\cdot(\mathrm{grad}(\delta T))\mathrm{d}V - \int_{\Gamma_O} s\delta T \,\mathrm{d}A + \int_{\Omega} r\delta T \,\mathrm{d}V, \tag{1}$$

where T is the temperature, ρ is the material density, $c_{\mathrm{p}}(T)$ the temperature dependent heat capacity, $\boldsymbol{\lambda}(T)$ is the temperature dependent thermal conductivity tensor, s is a surface flux at the boundary, and r is a heat flux source term. The surface flux s splits into two terms to account for convection as well as radiation ($s = s_{\mathrm{conv}} + s_{\mathrm{rad}}$), and the source term r can be used to account for latent heat. It can be assumed that the sintering of the powder bed, in particular, influences the heat conduction of the metal, in addition to the specific heat capacity, the radiation and convection effects. The correct modeling of heat conduction is therefore essential for the virtual design of the process control.

Phase state prediction

Xie et al. [8] and Zhang et al. [9] introduced the three phases powder, melt and solid in their work in the context of a process simulation of the PBF-LB/M and modeled the corresponding phase transitions. In their approach, which was implemented in the commercial FE software Abaqus, the described phase state was determined as a function of the current temperature and the temperature history according to Fig. 1. Where T_{S} is the solidus temperature and T_{L} is the liquidus temperature. In the temperature range $T_{\mathrm{S}} < T < T_{\mathrm{L}}$, the phase transition from the powder state to the melt takes place and transformation enthalpy resp. latent heat is released. The current phase was assigned a corresponding status variable (SDV) in an Abaqus user subroutine. [8, 9]

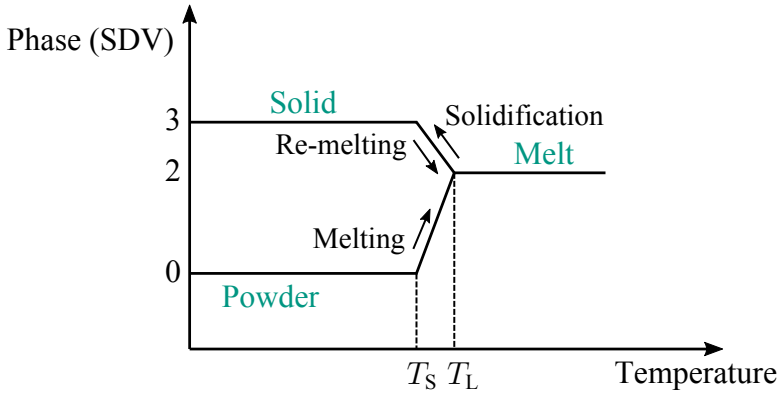

Fig. 1: Setting phase (represented in the form of state variables (SDV)) as a function of the locally occurring temperature. Consideration of the powder (0), melt (2) and solid (3) phases. [8, 9]

In order to define a range in which sintering takes place, the phase of the powder must be extended by another ”subphase”. Fig. 2 shows this extension. Once the sintering temperature T_{Sint} is reached, the powder is in the so-called sinter phase. In this temperature range between T_{Sint} and T_{L} local sintering effects occur in the powder bed and the degree of sintering increases. If T_{L} is not reached and the temperature drops below T_{Sint} again, the phase of pure powder is re-established. Thus, no further sintering

takes place and the degree of sintering remains constant. As soon as the T_L temperature of the metal is exceeded, the state can change between melt and solid depending on the prevailing temperature. In the presented work, transformation enthalpy is not considered so far. For this purpose, experimental investigations on the temperature range $T_\mathrm{S} < T < T_\mathrm{L}$, in which such an enthalpy is released, and how the sintering of the powder behaves in this range are missing. Therefore, T_S is not considered further in the following and T_L is assumed as the melting temperature.

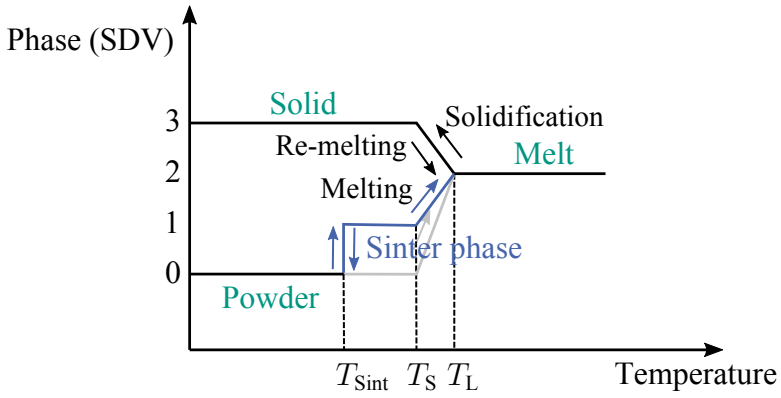

Fig. 2: Setting phase (represented in terms of state variables (SDV)) due to the local occurring temperature, taking into account the sinter phase.

Degree of sintering

The local degree of sintering is predicted by a sintering potential $\phi(\boldsymbol{X}, t)$ introduced by Kolossov et al. [7]. The physical model of the selectiv laser sintering (SLS) process presented by Kolossov et al. is based on the theory of continuous media. The sintering potential $\phi(\boldsymbol{X}, t)$ is defined at point $\boldsymbol{X}$ at time t as follows:

$$\phi(\boldsymbol{X}, t) = 1 - \exp\left(- \int_0^t \zeta(T(\boldsymbol{X}, \tau)) d\tau \right) \tag{2}$$

Where $\zeta(T(\boldsymbol{X}, \tau)$ represents the temperature-dependent sintering rate. $\phi(\boldsymbol{X}, t)$ contains information about the sintering state of the material. The range of values of ϕ is [0, 1). The value $\phi = 0$ corresponds to a loose powder, while ϕ takes the value 1 for fully sintered material. Since the data on molten metals are very sparse, Kolossev et al. proposed in [7] a piecewise linear model for the sintering rate:

$$\zeta(T) = \begin{cases} 0 & , T \leq T_\mathrm{Sint} \\ (T - T_\mathrm{Sint})/m & , T > T_\mathrm{Sint} \end{cases} \tag{3}$$

The fitting parameter m was first introduced in [7]. Kollosov et al. determined the parameter to be $m = 180$. The PBF-LB/M process generally has significantly shorter process times than the SLS process presented in [7]. Therefore, the calibration parameter in the simulation approach presented in this paper is changed according to the ratio of the process speed of the SLS process presented in [7] to the PBF-LB/M process speed assumed here to $m = 180/1000$.

Thermal parameters

In the real melting process of the powder, the enclosed air is released to the outside during the sintering and melting process. This leads to a change in the volume of the printed layer. However, this

volume change is not represented in the finite element model used in the work presented. This would require a continuous change in the local position of the following recoated powder layer. The volume of an element therefore remains the same in the simulation. It follows that, due to conservation of mass, the temperature-dependent density of the metal $\rho_{\mathrm{Al}}(T)$ is also constant during the phase transition. In addition, it follows from this that for reasons of energy conservation, the specific heat capacity $c_{\mathrm{p}}^{\mathrm{Al}}(T)$ must not change during the phase transition [10]. $c_{\mathrm{p}}^{\mathrm{Al}}(T)$ is therefore given as a function of temperature in all phases corresponding to the solid phase. Above T_{L} the heat capacity $c_{\mathrm{p}}^{\mathrm{Al}}(T)$ remains constant.

For the prediction of the temperature-dependent thermal conductivity of the powder bed $\boldsymbol{\lambda}_{\mathrm{PB}}(\boldsymbol{T})$ in the context of a PBF-LB/M simulation, different approaches were presented in the literature. Here, $\boldsymbol{\lambda}_{\mathrm{PB}}(\boldsymbol{T})$ are usually estimated with the scalar conductivity $\lambda_{\mathrm{PB}}(T)$ as isotropic and as a function of the porosity of the powder bed, taking into account that the powder consists of solid grains and a liquid material (gas). An overview of possible modeling approaches is given by Papazoglou et al. [11]. In the context of this publication, due to the missing experimental investigations of the present process, the approach of Yin et al. [12] is chosen for simplicity. In their work, a simplified relationship over the thermal conductivity of the powder bed is implemented as follows:

$$\lambda_{\mathrm{PB}}(T) = \lambda_{\mathrm{Solid}}(T)(1-\varphi)^{\alpha} \tag{4}$$

where $\lambda_{\mathrm{Solid}}(T)$ is the temperature dependent thermal conductivity of the solid, φ the porosity of loose powder and α an empirical coefficient defined in [12] as $\alpha = 4$.
To consider the changing thermal conductivity due to local sintering, Kolossov et al. [7] formulated $\lambda_{\mathrm{PB}}^{\mathrm{Sint}}(T)$ as a function of the sintering potential ϕ from Eq. 2 as follows:

$$\lambda_{\mathrm{PB}}^{\mathrm{Sint}}(T) = (a + (b-a)\phi)\lambda_{\mathrm{Solid}}(T) \tag{5}$$

Where $a > 0$ represents the ratio between the conductivity of loose powder and the solid conductivity $\lambda_{\mathrm{Solid}}(T)$ and $b > 0$ represents the ratio between the conductivity of completely sintered material ($\lambda_{\mathrm{PB}}^{\mathrm{Sint}}(T) = \lambda_{\mathrm{PB}}^{\mathrm{Sint}}(T)(\phi(\boldsymbol{X} = 1, t))$) and the solid conductivity $\lambda_{\mathrm{Solid}}(T)$.
Oriented to Fig. 2, the thermal conductivity coefficient can be formulated as follows until T_{L} is reached for the first time:

$$\lambda(T) = \begin{cases} (1-\varphi)^{\alpha}\lambda_{\mathrm{Solid}}(T) & , T \leq T_{\mathrm{Sint}} \\ (a + (b-a)\phi)\lambda_{\mathrm{Solid}}(T) & , T_{\mathrm{Sint}} < T \leq T_{\mathrm{L}} \\ \lambda_{\mathrm{Melt}}(T) & , T_{\mathrm{L}} < T \end{cases} \tag{6}$$

where $\lambda_{\mathrm{Melt}}(T)$ is the temperature dependent thermal conductivity of the melt pool. If the modeling approach presented in Eq. 4 is used for the formulation of the ratio a between the conductivity $\lambda_{\mathrm{PB}}(T)$ of loose powder and the solid conductivity $\lambda_{\mathrm{Solid}}(T)$, the following expression follows.

$$a = \frac{\lambda_{\mathrm{PB}}(T < T_{\mathrm{Sint}})}{\lambda_{\mathrm{Solid}}(T)} = \frac{(1-\varphi)^{\alpha}\lambda_{\mathrm{Solid}}(T)}{\lambda_{\mathrm{Solid}}(T)} = (1-\varphi)^{\alpha}. \tag{7}$$

Accordingly, the formulation of $\lambda(T)$ for temperatures up to the first exceeding of the melting temperature simplifies as follows:

$$\lambda(T) = \begin{cases} ((1-\varphi)^{\alpha} + (b-(1-\varphi)^{\alpha})\phi)\lambda_{\text{Solid}}(T) & ,T \leq T_{\text{L}} \\ \lambda_{\text{Melt}}(T) & ,T > T_{\text{L}} \end{cases} \tag{8}$$

The model parameter b is set to 0.6 according to [7] in this publication. After T_{L} is reached for the first time, the heat conduction can be assumed as follows:

$$\lambda(T) = \begin{cases} \lambda_{\text{Solid}}(T) & ,T \leq T_{\text{L}} \\ \lambda_{\text{Melt}}(T) & ,T > T_{\text{L}} \end{cases} \tag{9}$$

As already mentioned, the transformation enthalpy caused by the phase transitions is not considered. The transformation enthalpy can be taken into account subsequently in the existing model after corresponding experimental investigations, e.g. by the source term r or the change of the specific heat capacity c_{p}^{Al} [13].

Process Simulation PBF-LB/M

The presented modeling approach is implemented as user subroutine UMATHT for use in the commercial FE program Abaqus. A single bead test is modeled. The subroutines available in Abaqus for the simulation of additive manufacturing processes are used for element activation and the specification of a heat source to represent the energy input by the laser. The model structure with dimensions as well as the local discretization can be seen in Fig. 3.

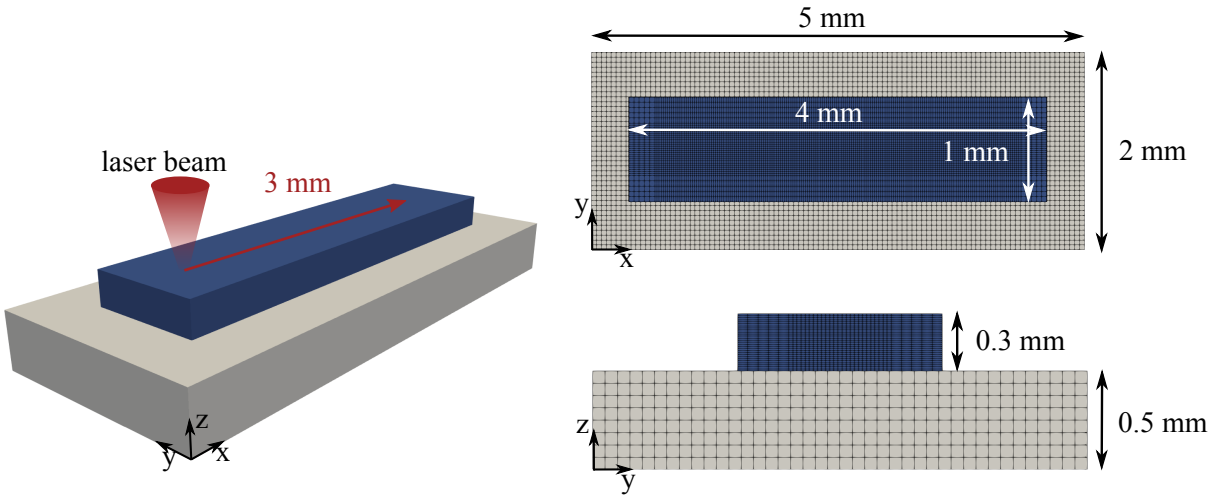

Fig. 3: Model setup and meshing of the single bead experiment. The six printing layers with a height of 0.05 mm each are shown in blue, the overprinted temperature-unstable material in gray.

Each of the six printed layers with a thickness of 0.05 mm is discretized with five elements in the thickness direction to also predict the change in sintering over the layer thickness. In the y-direction, the layers are discretized with elements of different edge lengths. In the energy input region, elements with an edge length of 0.05 mm are used. A Goldak heat source [14] is used to model the energy input. For the geometrical dimensions of the melt pool as well as the resulting sintering areas due to the energy input of the laser, no sufficient experimental investigations are available within the scope of the present work so far. Therefore, the geometry parameters for the Goldak heat source shown in Fig. 4 are determined by simulation to ensure a homogeneous temperature distribution over a sufficiently large

area. This enables an interpretable large sintering area. Simulative studies are also used to specify the laser powers that lead to sintering in the interfacial layers with the material and model parameters assumed here. A process velocity of $v = 1150\,\mathrm{mm/s}$ is used.

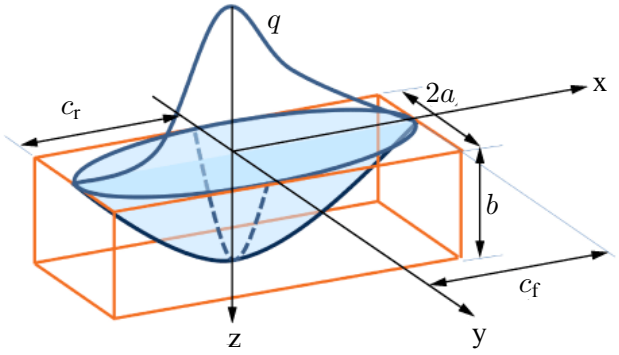

Fig. 4: The Goldak expression for the energy distribution, $q_{f/r} = \frac{6\sqrt{3} f_{f/r} Q}{abc\pi\sqrt{\pi}} e^{\left(-\frac{3x^2}{c^2_{f/r}}\right)} e^{\left(-\frac{3y^2}{a^2_2}\right)} e^{\left(-\frac{3z^2}{b^2_1}\right)}$, of a laser source. With $q = q_f$ when $x \geq 0$, $q = q_r$ when $x < 0$ and $f_f + f_r = 2$. The local x-axis indicates the direction of the laser motion [15].

The metal is modeled as AlSI10Mg as a function of temperature. The temperature-dependent material properties of the temperature-unstable material are based on an acrylonitrile-butadiene-styrene copolymer (ABS). The corresponding material properties are listed in Tab. 1 (AlSi10Mg) and Tab. 2 (ABS). In the implemented model, linear interpolation is used between the material parameters for a given temperature. Based on Nandy et al. [16], $T_{\mathrm{Sint}} = 527\,^{\circ}\mathrm{C}$ and $T_{\mathrm{L}} = 596\,^{\circ}\mathrm{C}$ were chosen. In addition, perfect thermal contact is assumed between the powder bed and the substrate, as well as between the powder bed or substrate and the overprinted temperature-unstable material.

In addition to the thermal approach presented in this work, the state-of-the-art modeling approach presented by, e.g., Xie et al. [8] and Zhang et al. [9]is also implemented in a UMATHT with the same material and process parameters, and used for comparison.

Table 1: Material parameters used for the simulation of AlSi10Mg.

AlSi10Mg (all phases)		
Convection heat transfer coefficient h_{Al} in $\mathrm{Wm^{-2}K^{-1}}$	18 [9]	
Emissivity $\varepsilon_{\mathrm{Al}}$ in $-$	0.36	
AlSi10Mg (Solid)	23 °C	596 °C
Density $\rho_{\mathrm{Al}}(T)$ in $\mathrm{kgm^{-3}}$	2740 [17]	2550 [17]
Thermal conductivity λ_{Solid} in $\mathrm{Wm^{-1}K^{-1}}$	155 [17]	165 [17]
Specific heat capacity $c_{\mathrm{p}}^{\mathrm{Al}}(T)$ in $\mathrm{Jkg^{-1}K^{-1}}$	750 [17]	1150 [17]
AlSi10Mg (Melt)	596 °C	2500 °C
Density $\rho_{\mathrm{Al}}(T)$ in $\mathrm{kgm^{-3}}$	2550 [17]	-
Thermal conductivity λ_{Melt} in $\mathrm{Wm^{-1}K^{-1}}$	85 [17]	110 [17]
Specific heat capacity $c_{\mathrm{p}}^{\mathrm{Al}}(T)$ in $\mathrm{Jkg^{-1}K^{-1}}$	1150 [17]	-

Table 2: Material parameters used for the simulation of ABS.

ABS	
Density $\rho_{\mathrm{ABS}}(T)$ in kgm^{-3}	1050.0 [18]
Thermal conductivity λ_{ABS} in $\mathrm{Wm}^{-1}\mathrm{K}^{-1}$	0.177 [18]
Specific heat capacity $c_{\mathrm{p}}^{\mathrm{ABS}}$ in $\mathrm{Jkg}^{-1}\mathrm{K}^{-1}$	2080.0 [18]
Convection heat transfer coefficient h_{ABS} in $\mathrm{Wm}^{-2}\mathrm{K}^{-1}$	80.0
Emissivity $\varepsilon_{\mathrm{ABS}}$ in $-$	0.96

Results and Discussion

The simulative investigations to determine the parameters for the Goldak heat source shown in Fig. 4 resulted in the parameters given in Tab. 3. Compared to the typical parameters of a Goldak heat source for the PBF-LB/M, large dimensions in width and depth of the heat source resulted. As a consequence, comparatively high laser powers have to be specified. To obtain interpretable sintering with the model and material parameters assumed here, a laser power of $550\,\mathrm{W}$ in the first layer and $460\,\mathrm{W}$ in the two following layers is required. After that, a laser power of $480\,\mathrm{W}$ is to be assumed and then increased by $10\,\mathrm{W}$ per layer. Furthermore, a recoating time of $0.1\,\mathrm{s}$ is set. This is sufficient to achieve adequate cooling of the print surface between printing layers with the given material data and model setup. With a time increment of $t_{\mathrm{inc}} = 0.0001\,\mathrm{s}$, the necessary computation time is also kept within acceptable limits. When choosing these process and model parameters, it should be noted that the chosen parameters are not subject to experimental investigations. To represent a realistic sintering process, experimental investigations must be carried out systematically and the material and model parameters determined accordingly. It can be assumed that for a realistic representation of the melt pool as well as the sintered areas, the choice of parameters for the Goldak heat source in the area of the interface must be different for each layer.

Table 3: Geometry parameters used for the Goldak heat source.

c_{r}	c_{f}	a	b	f_{r}	c_{f}
0.2	0.2	0.2	0.6	1.7	0.3

Fig. 5 a) shows the predicted solid fraction in green as well as the sintering potential in blue and red for the model extension presented in this publication. For the model approach according to [8, 9] Fig. 5 (b) shows the solid fraction in green and the powderbed in blue. Accordingly, the model extension presented here allows the prediction of sintered regions. In addition, the proportion of the solid phase is lower with the modified approach. Therefore, the heat dissipation in the area of energy input increases. If the subsequent layer is exposed, lower temperature leads to a smaller melt pool and thus to a reduced solid phase. The influence of sintering on the conductivity in the interfacial layers also affects the heat input into the temperature-unstable material. Fig. 6 shows the temperature in the ABS at the contact between metal and polymer over the processing time for both approaches. The temperatures deviate at higher process times, although with the process parameters chosen here the sintered region does not reach the contact. If sintering occurs up to the contact, it can be assumed that the influence on the temperature input will be even stronger. The presented results show that the sintering effects have to be considered to correctly predict the temperature input into the temperature-unstable material and the resulting solid fraction. Furthermore, the degree of sintering allows an evaluation of the mechanical properties of the resulting boundary layer after a thermal simulation. The presented approach can thus contribute to a fundamental understanding of process hybridization. For this purpose, however, the model parameters for the corresponding process have to be determined by experimental investigations.

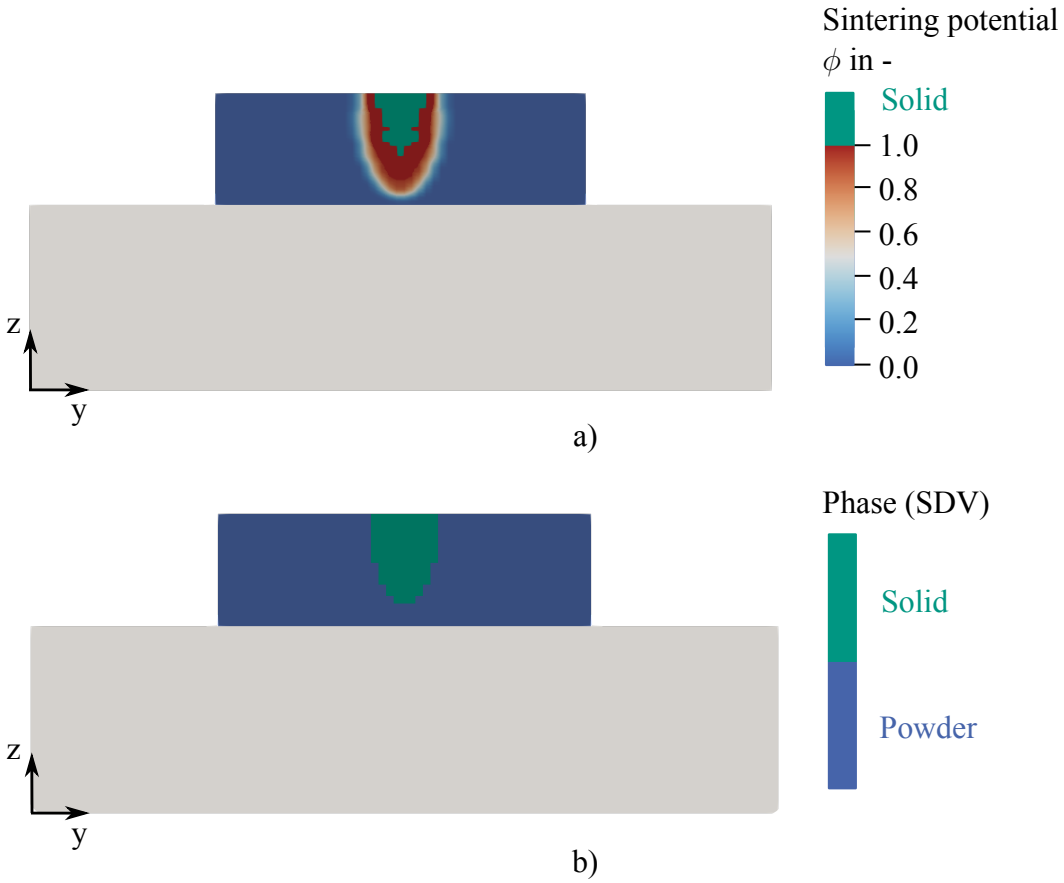

Fig. 5: Solid fraction in green as well as the sintering potential in blue and red for the model extension presented in this publication (a) and for the model approach according to [8, 9] (b).

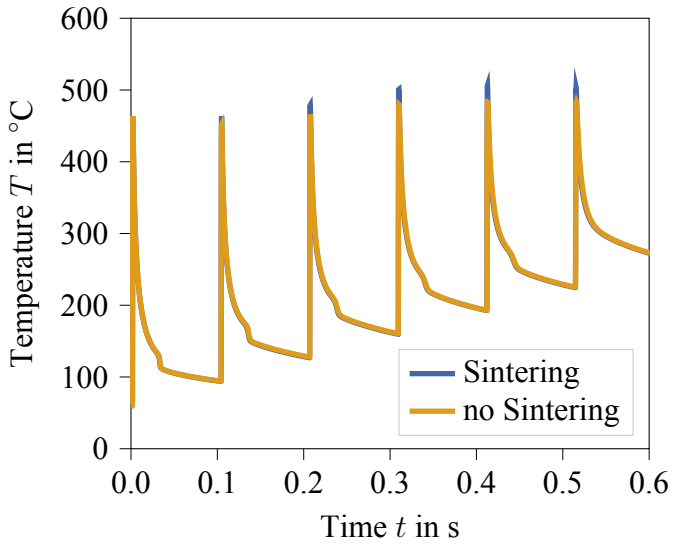

Fig. 6: Temperature in the ABS at the contact over the processing time t without consideration of sintering (yellow) and with addition of a sintering potential (blue).

Conclusion and Outlook

An approach for thermal modeling of Laser Powder Bed Fusion (PBF-LB/M) using relatively low laser powers is presented, which includes the prediction of sintering based on a sintering potential. This approach enables a process simulation of overprinting of temperature-unstable materials using the PBF-LB/M process. The increased thermal conductivity of the sintered material is taken into account. This allows a correct prediction of the temperature input into the temperature-unstable material. It was additionally shown that the consideration of sintering has an influence on the predicted solid fraction. Further, the modeling approach allows prediction of the mechanical properties of the resulting interfacial layer based on sintering in additional simulations.The presented approach can thus contribute to a fundamental understanding of process hybridization.

To predict the temperature history even better, the resulting transformation enthalpy must also be included both during sintering and during phase transformation. However, this requires experimental investigations to be carried out in advance to determine the enthalpy generated during the sintering process. It has to be considered that the selected model parameters for determining the degree of sintering and the thermal conductivity as well as selected process and material parameters are not based on experimental investigations. To represent a realistic sintering process, experimental investigations must be carried out systematically and the material and model parameters determined accordingly.

Acknowledgements

The project, which the presented work is carried out for, was funded through the EXU Measure KIT Future Fields project Hybrid^2-PaM. The authors thank Kai Uwe Drechsel for fruitful discussions. The work is also part of the Young Investigator Group (YIG) “Tailored Composite Materials for Lightweight Vehicles”, generously funded by the Vector Stiftung.

References

[1] D. D. Gu, W. Meiners, K. Wissenbach, and R. Poprawe, “Laser additive manufacturing of metallic components: Materials, processes and mechanisms,” *International Materials Reviews*, vol. 57, no. 3, pp. 133–164, 2012.

[2] R. H. Morgan, A. J. Papworth, C. Sutcliffe, P. Fox, and W. O’Neill, “High density net shape components by direct laser re-melting of single-phase powders,” *Journal of Materials Science*, vol. 37, no. 15, pp. 3093–3100, 2002.

[3] S. Merkt, C. Hinke, H. Schleifenbaum, and H. Voswinckel, “Geometric complexity analysis in an integrative technology evaluation model (ITEM) for selective laser melting (SLM),” *South African Journal of Industrial Engineering*, vol. 23, no. July, pp. 97–105, 2012.

[4] Y.-H. Chueh, C. Wei, X. Zhang, and L. Li, “Integrated laser-based powder bed fusion and fused filament fabrication for three-dimensional printing of hybrid metal/polymer objects,” *Additive Manufacturing*, vol. 31, p. 100928, 2020.

[5] S.-H. Tang, C.-W. Cheng, R.-Y. Yeh, and R.-Q. Hsu, “Direct joining of 3D-printed thermoplastic parts to SLM-fabricated metal cellular structures by ultrasonic welding,” *The International Journal of Advanced Manufacturing Technology*, vol. 99, no. 1, pp. 729–736, 2018.

[6] G. Lucchetta, F. Marinello, and P. Bariani, “Aluminum sheet surface roughness correlation with adhesion in polymer metal hybrid overmolding,” *CIRP annals*, vol. 60, no. 1, pp. 559–562, 2011.

[7] S. Kolossov, E. Boillat, R. Glardon, P. Fischer, and M. Locher, "3D FE simulation for temperature evolution in the selective laser sintering process," *International Journal of Machine Tools and Manufacture*, vol. 44, no. 2-3, pp. 117–123, 2004.

[8] J. Xie and J. A. Hurtado, "Phase Transformations in Metals during Additive Manufacturing Processes Frictional stability View project Additive Manufacturing Process Simulation View project," *NAFEMS World Congress 2017*, no. August, 2017.

[9] Q. Zhang, J. Xie, Z. Gao, T. London, D. Griffiths, and V. Oancea, "A metallurgical phase transformation framework applied to SLM additive manufacturing processes," *Materials and Design*, vol. 166, 2019.

[10] N. Keller, *Nils Keller Verzugsminimierung bei selektiven Laserschmelz- verfahren durch Multi-Skalen-Simulation*. PhD thesis, Universität Bremen, 2017.

[11] E. L. Papazoglou, N. E. Karkalos, P. Karmiris-Obratański, and A. P. Markopoulos, "On the Modeling and Simulation of SLM and SLS for Metal and Polymer Powders: A Review," *Archives of Computational Methods in Engineering*, no. 0123456789, 2021.

[12] J. Yin, H. Zhu, L. Ke, W. Lei, C. Dai, and D. Zuo, "Simulation of temperature distribution in single metallic powder layer for laser micro-sintering," *Computational Materials Science*, vol. 53, no. 1, pp. 333–339, 2012.

[13] R. B. Patil and V. Yadava, "Finite element analysis of temperature distribution in single metallic powder layer during metal laser sintering," *International Journal of Machine Tools and Manufacture*, vol. 47, no. 7-8, pp. 1069–1080, 2007.

[14] J. Goldak, A. Chakravarti, and M. Bibby, "A New Finite Element Model for Welding Heat Sources," *METALLURGICAL TRANSACTIONS B*, vol. 15B, pp. 299–305, 1983.

[15] *ABAQUS/Standard User Assistance R2021x*. Providence, RI, USA: Dassault Systemes Simulia Corp, 2020.

[16] J. Nandy, N. Yedla, P. Gupta, H. Sarangi, and S. Sahoo, "Sintering of AlSi10Mg particles in direct metal laser sintering process: A molecular dynamics simulation study," *Materials Chemistry and Physics*, vol. 236, no. June, p. 121803, 2019.

[17] C. Liu, C. Li, Z. Zhang, S. Sun, M. Zeng, F. Wang, Y. Guo, and J. Wang, "Modeling of thermal behavior and microstructure evolution during laser cladding of AlSi10Mg alloys," *Optics and Laser Technology*, vol. 123, no. August, p. 105926, 2020.

[18] C. Bellehumeur, L. Li, Q. Sun, and P. Gu, "Modeling of bond formation between polymer filaments in the fused deposition modeling process," *Journal of Manufacturing Processes*, vol. 6, no. 2, pp. 170–178, 2004.